



The Formation Conditions of Chondrules and Chondrites

C. M. O'D. Alexander, *et al.*
Science **320**, 1617 (2008);
DOI: 10.1126/science.1156561

The following resources related to this article are available online at www.sciencemag.org (this information is current as of June 20, 2008):

Updated information and services, including high-resolution figures, can be found in the online version of this article at:

<http://www.sciencemag.org/cgi/content/full/320/5883/1617>

Supporting Online Material can be found at:

<http://www.sciencemag.org/cgi/content/full/320/5883/1617/DC1>

This article appears in the following **subject collections**:

Geochemistry, Geophysics

http://www.sciencemag.org/cgi/collection/geochem_phys

Information about obtaining **reprints** of this article or about obtaining **permission to reproduce this article** in whole or in part can be found at:

<http://www.sciencemag.org/about/permissions.dtl>

from the source to the measurement (fig. S2). The result (purple dashed line in Fig. 4B) is compared with the intrinsic attosecond chirp (green solid line in Fig. 4B) calculated from a classical trajectory analysis (23, 24). There is a notable discrepancy at the high-energy components of the wave packet, possibly because of quantum effects near cutoff. Nevertheless, the agreement with the attochirp resulting from short trajectories is stunning in the main part of the spectrum, where the S/N ratio is excellent. This agreement indicates the powerfulness of semiclassical modeling of strong-field interactions (25, 26) and the negligible role of long trajectories in contributing to the XUV radiation in the far field (27).

In a similar way, the confinement of interaction between the ionizing field and the atom to a single wave cycle will permit accurate quantitative tests of theories of strong-field ionization. The sub-100-as XUV pulses emerging from the interaction with a flux greater than 10^{11} photons/s—along with their monocycle NIR driver wave—will push the resolution limit of attosecond spectroscopy to the atomic unit of time (~ 24 as) and allow for the real-time observation of electron correla-

tions, by means of streaking (6), tunneling (14), or absorption (28) spectroscopy.

References and Notes

1. A. Baltuska *et al.*, *Nature* **421**, 611 (2003).
2. R. Kienberger *et al.*, *Nature* **427**, 817 (2004).
3. E. Goulielmakis *et al.*, *Science* **305**, 1267 (2004).
4. M. F. Kling *et al.*, *Science* **312**, 246 (2006).
5. G. Sansone *et al.*, *Science* **314**, 443 (2006).
6. A. L. Cavalieri *et al.*, *Nature* **449**, 1029 (2007).
7. E. Goulielmakis *et al.*, *Science* **317**, 769 (2007).
8. S. Svensson, B. Eriksson, N. Martensson, G. Wendin, U. J. Gelius, *J. Electron Spectrosc. Relat. Phenom.* **47**, 327 (1988).
9. S. X. Hu, L. A. Collins, *Phys. Rev. Lett.* **96**, 073004 (2006).
10. J. Breidbach, L. S. Cederbaum, *Phys. Rev. Lett.* **94**, 033901 (2005).
11. A. I. Kuleff, J. Breidbach, L. S. Cederbaum, *J. Chem. Phys.* **123**, 044111 (2005).
12. F. Remacle, R. D. Levine, *Proc. Natl. Acad. Sci. U.S.A.* **103**, 6793 (2006).
13. G. Yudin, M. Y. Ivanov, *Phys. Rev. A* **64**, 035401 (2001).
14. M. Uiberacker *et al.*, *Nature* **446**, 627 (2007).
15. T. Pfeifer *et al.*, *Phys. Rev. Lett.* **97**, 163901 (2006).
16. Y. Oishi *et al.*, *Opt. Express* **14**, 7230 (2006).
17. See supporting material on Science Online.
18. C. A. Haworth *et al.*, *Nature Phys.* **3**, 52 (2007).
19. A. L. Cavalieri *et al.*, *New J. Phys.* **9**, 242 (2007).
20. R. Trebino, D. J. Kane, *J. Opt. Soc. Am. A* **10**, 1101 (1993).
21. Y. Mairesse, F. Quéré, *Phys. Rev. A* **71**, 011401(R) (2005).
22. D. J. Kane, G. Rodriguez, A. J. Taylor, T. S. Clement, *J. Opt. Soc. Am. B* **14**, 935 (1997).
23. P. Salières *et al.*, *Science* **292**, 902 (2001).
24. V. S. Yakovlev, A. Scrinzi, *Phys. Rev. Lett.* **91**, 153901 (2003).
25. P. B. Corkum, *Phys. Rev. Lett.* **71**, 1994 (1993).
26. K. J. Schafer, B. Yang, L. F. DiMauro, K. C. Kulander, *Phys. Rev. Lett.* **70**, 1599 (1993).
27. R. López-Martens *et al.*, *Phys. Rev. Lett.* **94**, 033001 (2005).
28. Z.-H. Loh *et al.*, *Phys. Rev. Lett.* **98**, 143601 (2007).
29. K. Varjú *et al.*, *Laser Phys.* **15**, 888 (2005).
30. Supported by the Max Planck Society and the Deutsche Forschungsgemeinschaft Cluster of Excellence: Munich Centre for Advanced Photonics (www.munich-photonics.de). E.G. acknowledges a Marie-Curie fellowship (MEIF-CT-2005-02440) and a Marie-Curie Reintegration grant (MERG-CT-2007-208643). A.L.A. is supported by the NSF Extreme Ultraviolet Engineering Research Center. R.K. acknowledges support from the Sofia Kovalevskaya award of the Alexander von Humboldt Foundation.

Supporting Online Material

www.sciencemag.org/cgi/content/320/5883/1614/DC1

SOM Text

Figs. S1 to S4

References

17 March 2008; accepted 27 May 2008

10.1126/science.1157846

The Formation Conditions of Chondrules and Chondrites

C. M. O'D. Alexander,^{1*} J. N. Grossman,² D. S. Ebel,³ F. J. Ciesla¹

Chondrules, which are roughly millimeter-sized silicate-rich spherules, dominate the most primitive meteorites, the chondrites. They formed as molten droplets and, judging from their abundances in chondrites, are the products of one of the most energetic processes that operated in the early inner solar system. The conditions and mechanism of chondrule formation remain poorly understood. Here we show that the abundance of the volatile element sodium remained relatively constant during chondrule formation. Prevention of the evaporation of sodium requires that chondrules formed in regions with much higher solid densities than predicted by known nebular concentration mechanisms. These regions would probably have been self-gravitating. Our model explains many other chemical characteristics of chondrules and also implies that chondrule and planetesimal formation were linked.

Chondrules make up ~ 20 to 80 volume % of most chondrites and formed at peak temperatures of ~ 1700 to 2100 K (1). Chondrules in the different chondrite groups have distinct physical and chemical properties (2), as well as distinct age ranges (3), indicating that they formed in relatively local environments via a process that operated at least periodically between ~ 1 and 4 million years after the formation of the solar system.

It was long thought that individual chondrules behaved as chemically closed systems during their formation, inheriting their compositions from their precursors (4, 5). However, for likely cooling rates of 10 to 1000 K/hour (1) and at the low pressures

(total pressure $\approx 10^{-6}$ to 10^{-3} bars) of the solar protoplanetary disk (nebula), experiments (6–8), natural analogs (9, 10), and theoretical calculations (11, 12) all show that there should be extensive evaporation of major and minor elements, in the order $S > Na, K > Fe > Si > Mg$.

Elemental fractionations in chondrules are generally a function of volatility (4, 5). If evaporation in the nebula produced the alkali metal and Fe fractionations, the more volatile elements (such as S) should be entirely absent, which they are not. In addition, the fractionated elements should exhibit large and systematic isotopic fractionations, which they do not (13).

Here we demonstrate that chondrules did indeed behave as essentially closed systems during melting, at least for elements with volatilities less than or equal to that of Na. We also propose a means of resolving the apparent conflict between this result and experimental and theoretical expecta-

tations that chondrules should have suffered considerable evaporation during formation. Our conclusions have implications for mechanisms of dust concentration in the solar nebula, for chondrule formation, and for planetesimal formation.

Chondrules are dominated by olivine [(Mg,Fe)₂SiO₄], pyroxene [(Mg,Fe,Ca)SiO₃], Fe-Ni metal, and quenched silicate melt (glass). Many of the more volatile elements (such as Na) can diffuse rapidly, particularly in melts and glasses. Therefore, it is possible that volatiles were completely lost when chondrules melted, and reentered the chondrules during cooling or even after solidification. However, Na clinopyroxene/glass ratios show that the Na contents of the final chondrule melts (now glass) had approximately their observed, relatively high abundances at temperatures of ~ 1600 to 1200 K (14–16).

Calculations suggest that chondrule melts could have been stabilized in the nebula by substantially enriching solids (chondrule precursors or other dust) relative to gas (11, 12). This also substantially increases the condensation temperatures of even highly volatile elements such as S (11, 12). Even in solid-enriched systems, there is an initial phase of evaporation when a chondrule melts, but subsequent chondrule/gas re-equilibration would erase any isotopic fractionations (12). If the enrichment of solids is high, little evaporation may be needed to reach chondrule/gas equilibrium, and the behavior of volatile elements during cooling would resemble closed-system behavior. However, even at a high total pressure of 10^{-3} bars, with a solids enrichment of 1000 relative to the solar composition, all the Na would evaporate at near-liquidus temperatures, and substantial recondensation only begins well below 1600 K (11). Locally enriching chondrule-sized or smaller solids by 1000 times

¹Department of Terrestrial Magnetism, Carnegie Institution of Washington, Washington, DC 20015, USA. ²U.S. Geological Survey, Reston, VA 20192, USA. ³American Museum of Natural History, New York, NY 10024, USA.

*To whom correspondence should be addressed. E-mail: alexande@dtm.ciw.edu

on substantial spatial scales would have been difficult to achieve in the nebula with known mechanisms (17), except perhaps if levels of turbulence were very low (18).

It is evident from the above that the behavior of Na during cooling can constrain the degree to which solids were enriched during chondrule formation. Olivine is the highest-temperature liquidus phase in chondrules and is predicted to crystallize throughout much of their supersolidus cooling (11). Olivine phenocrysts in chondrules are generally zoned in major and minor elements, demonstrating that olivine cores did not maintain equilibrium with the liquid during cooling. Na does partition into olivine, albeit at low levels. Therefore, if Na could be measured in them, olivine phenocrysts should record any changes in the Na content of their host chondrules as they crystallized.

We analyzed bulk, mineral, and glass compositions in 26 Semarkona (classified as a LL3.0) chondrules (Table 1) (18) with a range of types (IA-IAB and IIA-IIAB-IIB, where I = FeO-poor, II = FeO-rich, A = olivine-dominated, B = pyroxene-dominated, and AB = intermediate). In general, chondrule olivines exhibit pronounced

normal zoning in major (Mg and Fe) and minor (Na, Cr, Mn, and Ca) elements that is consistent with expectations for crystallization from their bulk chondrule melts (5, 16, 19). Na can diffuse rapidly in some minerals and glasses at high temperature, but the fact that its zoning roughly parallels that of Cr, Mn, and Ca demonstrates its primary nature. In addition, the shapes of Na zoning profiles around Na- and Fe-poor relict olivine grains (unmelted precursors) (20, 21) in type II chondrules are similar to or broader than those of Fe (22), suggesting that Na diffusion rates in these olivines were comparable to those of Fe. Except where grains are clearly relict, analyses of phenocrysts and microphenocrysts from the same chondrule fall on similar trends, but these trends commonly differ from chondrule to chondrule.

The simple observation of measurable Na in the cores of chondrule olivines (Fig. 1 and Table 1) (18) is contrary to predictions (Fig. 1), even in what has previously been considered a highly dust-enriched system (1000 times that of the solar composition) (11). To determine how much Na was present in the chondrule melts during olivine crystallization, it is necessary to know the Na

olivine-melt distribution coefficient (K_D), measurements of which have yet to be published. However, clinopyroxene-glass partitioning demonstrates that the Na contents of the glass in the central regions of these chondrules were established before solidification (14–16). In olivine-normative chondrules, olivine was generally still on the liquidus at the onset of clinopyroxene crystallization [calculated with MELTS (23)]. Consequently, we can estimate the olivine-liquid K_D for Na at the end of crystallization for each chondrule as the ratio of the Na_2O contents of the last olivine to form (the most Na- and Fe-rich phenocryst rims and microphenocrysts) to that in the glass (rim K_{DS} , Table 1). The rim K_{DS} are fairly similar for all chondrules, implying no strong compositional dependence.

To determine whether bulk chondrule Na abundances were very different at liquidus

Table 1. The petrologic types and estimated liquidus temperatures of the Semarkona chondrules studied, as well as the Mg number and Na olivine-melt K_{DS} of the first (core) and last (rim) olivines to crystallize.

Chondrule	Type	Liquidus* (°C)	Core† Mg no.	Rim‡ Mg no.	Core§ K_D	Rim K_D	Density¶ (g/m ³)
C1	IIA	1680	0.898	0.699	0.0077(11)	0.0068(13)	17 to 311
C2	IIA	1652	0.888	0.796	0.0028(07)	0.0028(06)	12 to 194
C3	IIA	1658	0.898	0.716	0.0095(13)	0.0063(02)	14 to 251
C4	IIA	1702	0.905	0.771	0.0074(15)	0.0061(07)	33 to 476
C5	IIA	1646	0.792	0.722	0.015(02)	0.0053(09)	14 to 229
C6	IA‡#	1706	0.994	0.995	0.019(05)	0.0055(45)	91 to 2510
C7	IA	1716	0.996	0.994	0.0011(14)	0.0023(12)	51 to 1610
C8	IAB‡	1752	0.994	0.994	0.0066(44)	0.0025(12)	118 to 3090
C9	IAB‡	1770	0.993	0.993	0.025(13)	0.0081(40)	198 to 5750
C10	IIA	1642	0.791	0.791	0.0061(08)	0.0061(08)	11 to 194
C11	IA‡	1778	0.993	0.992	0.069(18)	0.0063(42)	388 to 9080
C13	IIAB	1582	0.846	0.647	0.0028(05)	0.0046(03)	3 to 60
C14	IIA	1672	0.909	0.675	0.0032(07)	0.0041(05)	16 to 260
C18	IIAB	1646	0.840	0.766	0.0031(06)	0.0020(02)	10 to 165
C19	IIAB	1630	0.936	0.888	0.0009(06)	0.0009(01)	6 to 117
C20	IIA	1718	0.923	0.795	0.0040(09)	0.0030(05)	32 to 526
C22	IIA	1678	0.910	0.688	0.0057(09)	0.0054(05)	15 to 273
C23	IIAB	1634	0.875	0.690	0.0014(06)	0.0031(04)	10 to 158
C27	IIAB	1674	0.875	0.780	0.0060(11)	0.0014(02)	14 to 259
C29	IIAB	1612	0.871	0.840	0.0009(05)	0.0003(01)	6 to 99
C31	IIAB	1630	0.849	0.696	0.0059(10)	0.0020(01)	7 to 128
C33	IIA#	1632	0.854	0.806	0.0024(06)	0.0027(01)	9 to 167
C34	IIAB	1554		0.738		0.0033(08)	2 to 43
C35	IIA	1580	0.835	0.745	0.0057(07)	0.0047(02)	4 to 72
C38	IIA	1704	0.866	0.813	0.0034(10)	0.0027(02)	30 to 534
C40	IIB	1622	0.858		0.0056(20)		6 to 139

*Liquidus temperatures were estimated with MELTS (23). †Mg number is the atomic Mg/(Mg+Fe) number of the olivine. ‡The alkali metals in the glasses of these chondrules are radially zoned. The core glass compositions were used for the rim K_{DS} and to calculate the initial bulk compositions. §The errors are based only on the uncertainty of the Na measurements in the olivine cores and a nominal 10% error in the bulk compositions. ||The errors are based only on uncertainties in the measured olivine and glass compositions. ¶Upper and lower density limits assume that 90% of the Na remained condensed. The lower limit assumes a vapor in equilibrium with a silicate melt only. The upper limit assumes a vapor in equilibrium with silicate and pure Fe-metal melts. #All chondrules have porphyritic textures, except C6 and C33, which are barred.

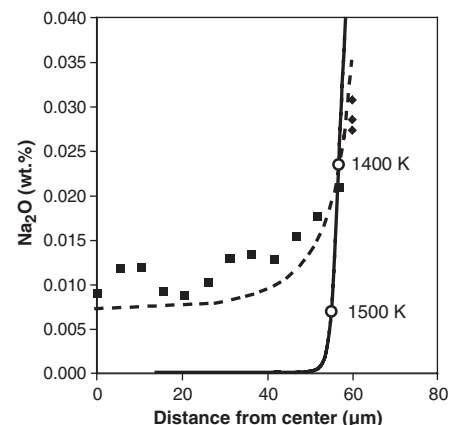


Fig. 1. Comparison of the Na_2O radial zonation in an olivine phenocryst (squares) from chondrule C3 with predictions (18) for closed-system crystallization (dashed line) and a chondrule forming in a region of the nebula with a total pressure of 10^{-3} bars that is enriched in solids relative to a solar gas by a factor of 1000 (solid line). wt %, weight %. The predictions assume an olivine-melt K_D of 0.0075 (Table 1). The diamond symbols represent microphenocrysts in the glass that probably most closely reflect the compositions of the last olivine to be in equilibrium with the glass.

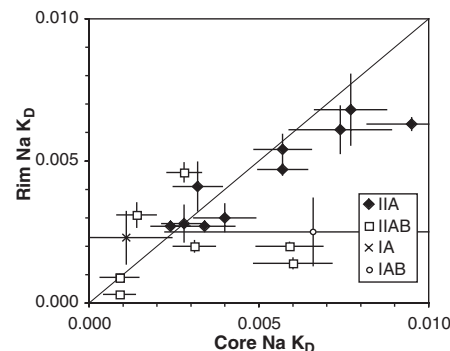


Fig. 2. The initial (core) and final (rim) olivine $\text{Na } K_D$ s for most of the Semarkona chondrules studied (Table 1). Four chondrules with large core K_{DS} fall outside the figure.

temperatures, when olivine began to grow (~400 to 500 K above the clinopyroxene and final olivine crystallization temperatures), we calculated the apparent K_{DS} for the cores of olivine grains. We did this for each chondrule, using their most Na- and Fe-poor core olivine compositions and their bulk Na content (core K_{DS} , Table 1). Figure 2 compares the apparent core and rim K_{DS} s. Most chondrules fall close to the 1:1 line, as would be expected for closed-system behavior. The notable exceptions, which all fall well to the right of the 1:1 line and out of the figure, are the three type IAs and chondrule C5, which have very high core K_{DS} . We suspect that this is because they contain unrecognized relatively Na-rich relict cores. The good correspondence between core and rim K_{DS} s for most chondrules, which cover several hundred degrees of cooling, suggests that (i) they do not have strong temperature or compositional dependences, and (ii) the Na contents of most chondrules did not vary dramatically during cooling. This inference is supported by the subparallel Na, Cr, Mn, and Ca zoning profiles in most olivine phenocrysts. Some chondrules do have core K_{DS} s that, for the quoted errors, are significantly lower than the rim K_{DS} s, which could be indicative of some Na gain by the melt during cooling, although the differences are still much less than predicted by the most solids-enriched model of (11).

There are several potential sources of uncertainty in estimating the K_{DS} s that could not be quantified (18). There is also a range of K_{DS} s even for those chondrules that lie close to the 1:1 line. Some of this variation could be due to the gain or loss of Na after crystallization (18). Despite these concerns, because most chondrules fall close to the 1:1 line, we infer that to first order they were essentially closed systems for Na during crystallization.

There is some uncertainty about the nebular conditions during chondrule formation. To estimate the range of solids densities that would have been necessary for roughly closed-system behavior of Na at liquidus temperatures, we calculated the equilibrium vapor pressures over the bulk chondrule silicate melts alone as well as over the silicate melts in equilibrium with pure Fe metal (18). The solids densities were estimated by calculating, for a given temperature and equilibrium pressure of Na (P_{Na}), the density of solids required for 90% of the Na to remain condensed (Table 1). If the P_{H_2} was $>10^{-7}$ bars during chondrule formation, it will increase the lower limits on the densities (18).

The ranges of solids densities in Table 1 are much higher than previously considered for chondrule formation. In principle, the required solids densities could be lowered if the oxygen fugacity (f_{O_2}) were enhanced. However, the f_{O_2} levels in the calculations of the lower limits were well above the iron-wüstite buffer and, therefore, almost certainly already too high because chondrules contain metal. The apparent absence of chondrules exhibiting clear evidence for the open-system behavior of Na or isotopic evidence

for evaporation indicates that the chondrules in chondrites formed almost exclusively in such high-density regions. Either there was a remarkably efficient process for concentrating chondrule precursors in regions with high solids densities, or only chondrules that formed in high-density regions accreted into chondrites.

On the basis of the lack of isotopic fractionations in chondrules, it has been estimated that chondrule-forming regions were at least 150 to 6000 km in radius (24). At the minimum liquidus densities we calculated (typically >10 g/m³), regions >4000 km in radius will be self-gravitating (18). Regions of this size and density should cool at rates that are consistent with those inferred for chondrules (18) and contain enough mass to produce a body of the size typically assumed for the chondrite parent asteroids (radius ~50 km, density ~3 g/cc). These observations raise the possibility that planetesimal formation and chondrule formation in high-density regions were linked. In any case, such high densities would promote the aggregation of larger objects that could then coalesce into asteroid-sized objects (25).

A close link between chondrule and planetesimal formation would explain how distinct chondrule populations were preserved in a turbulent nebula in which large-scale mixing would have occurred relatively rapidly. At near liquidus temperatures and inferred densities, there would be gas-mediated exchange between chondrules in close proximity to one another. The diversity of chondrule compositions would thus seem to be problematic, but equilibration time scales are poorly understood and would depend on vapor pressures, diffusion rates in the melts, and the magnitude of the initial compositional differences between chondrules. Even at equilibrium, differences in bulk chondrule compositions are possible to generate simply by varying the proportions of the equilibrium phases. The finite time scales of gaseous diffusion mean that if chondrule-forming regions were relatively large, microenvironments could exist within them (24). However, chondrite formation cannot have immediately followed chondrule formation, because at least some chondrules experienced multiple heating events (2), and the low-temperature matrix that cements chondrites must also be present before final assembly (18).

Shock (26) and current-sheet (27) heating models both predict thermal histories that are consistent with those inferred for chondrules. The solids densities we estimate are much higher than assumed in previous models (26, 27) but are more consistent with shock heating than with current sheets. Over the range of previously explored solids densities, chondrule cooling rates after shock heating are predicted to increase with increasing solids density. It remains to be seen whether the calculated cooling rates at the densities we estimate are consistent with those inferred for real chondrules. If not, other heating mechanisms, such as lightning or planetesimal collisions, will have to be explored.

References and Notes

- R. H. Hewins, H. C. Connolly Jr., G. E. Lofgren, G. Libourel, in *Chondrites and the Protoplanetary Disk*, A. N. Krot, E. R. D. Scott, B. Reipurth, Eds. (Astronomical Society of the Pacific, San Francisco, 2005), vol. 341, pp. 286–316.
- R. H. Jones, J. N. Grossman, A. E. Rubin, in *Chondrites and the Protoplanetary Disk*, A. N. Krot, E. R. D. Scott, B. Reipurth, Eds. (Astronomical Society of the Pacific, San Francisco, 2005), vol. 341, pp. 251–285.
- N. T. Kita *et al.*, in *Chondrites and the Protoplanetary Disk*, A. N. Krot, E. R. D. Scott, B. Reipurth, Eds. (Astronomical Society of the Pacific, San Francisco, 2005), vol. 341, pp. 558–587.
- J. N. Grossman, J. T. Wasson, in *Chondrules and their Origins*, E. A. King, Ed. (Lunar and Planetary Institute, Houston, TX, 1983), pp. 88–121.
- R. H. Jones, *Geochim. Cosmochim. Acta* **54**, 1785 (1990).
- Y. Yu, R. H. Hewins, C. M. O'D. Alexander, J. Wang, *Geochim. Cosmochim. Acta* **67**, 773 (2003).
- J. Wang, A. M. Davis, R. N. Clayton, T. K. Mayeda, A. Hashimoto, *Geochim. Cosmochim. Acta* **65**, 479 (2001).
- B. Cohen, R. H. Hewins, C. M. O'D. Alexander, *Geochim. Cosmochim. Acta* **68**, 1661 (2004).
- C. M. O'D. Alexander, S. Taylor, J. S. Delaney, P. Ma, G. F. Herzog, *Geochim. Cosmochim. Acta* **66**, 173 (2002).
- S. Taylor *et al.*, *Geochim. Cosmochim. Acta* **69**, 2647 (2005).
- D. S. Ebel, L. Grossman, *Geochim. Cosmochim. Acta* **64**, 339 (2000).
- C. M. O'D. Alexander, *Geochim. Cosmochim. Acta* **68**, 3943 (2004).
- A. M. Davis, C. M. O'D. Alexander, H. Nagahara, F. M. Richter, in *Chondrites and the Protoplanetary Disk*, A. N. Krot, E. R. D. Scott, B. Reipurth, Eds. (Astronomical Society of the Pacific, San Francisco, 2005), vol. 341, pp. 432–455.
- C. M. O'D. Alexander, J. N. Grossman, *Meteorit. Planet. Sci.* **40**, 541 (2005).
- G. Libourel, A. N. Krot, I. Tissandier, *Lunar Planet. Sci. XXXIV*, 1558 (abstr.) (2003).
- R. H. Jones, *Geochim. Cosmochim. Acta* **58**, 5325 (1994).
- J. N. Cuzzi, R. C. Hogan, J. M. Paque, A. R. Dobrovolskis, *Astrophys. J.* **546**, 496 (2001).
- Materials and methods are available as supporting material on Science Online.
- R. H. Jones, G. E. Lofgren, *Meteoritics* **28**, 213 (1993).
- H. Nagahara, *Nature* **292**, 135 (1981).
- R. H. Jones, in *Chondrules and the Protoplanetary Disk*, R. H. Hewins, R. H. Jones, E. R. D. Scott, Eds. (Cambridge Univ. Press, Cambridge, 1996), pp. 163–172.
- C. M. O'D. Alexander, J. N. Grossman, D. Ebel, *Lunar Planet. Sci. XXXVIII*, (2007).
- M. S. Ghiorso, R. O. Sack, *Contrib. Mineral. Petrol.* **119**, 197 (1995).
- J. N. Cuzzi, C. M. O'D. Alexander, *Nature* **441**, 483 (2006).
- A. Johansen *et al.*, *Nature* **448**, 1022 (2007).
- S. J. Desch, F. J. Ciesla, L. L. Hood, T. Nakamoto, in *Chondrites and the Protoplanetary Disk*, A. N. Krot, E. R. D. Scott, B. Reipurth, Eds. (Astronomical Society of the Pacific, San Francisco, 2005), vol. 341, pp. 849–872.
- M. K. R. Jong, M.-M. Mac Low, D. S. Ebel, *Astrophys. J.* **606**, 532 (2004).
- This paper is dedicated to the memory of Robert Hutchison. J. Nuth and an anonymous reviewer greatly improved this manuscript. C.A. was partially supported by NASA Origins of Solar Systems grant NNG06GE39G. J.G. was partially supported by NASA Cosmochemistry grant NNH05AB651, D.E. was partially supported by NASA Cosmochemistry grant NANG06GD89G, and F.C. was funded by a Department of Terrestrial Magnetism Carnegie Institution of Washington postdoctoral fellowship.

Supporting Online Material

www.sciencemag.org/cgi/content/full/320/5883/1617/DC1
Methods
Fig. S1
Tables S1 to S5
References

15 February 2008; accepted 14 May 2008
10.1126/science.1156561



Supporting Online Material for

The Formation Conditions of Chondrules and Chondrites

C. M. O'D. Alexander,* J. N. Grossman, D. S. Ebel, F. J. Ciesla

*To whom correspondence should be addressed. E-mail: alexande@dtm.ciw.edu

Published 20 June 2008, *Science* **320**, 1617 (2008)

DOI: 10.1126/science.1156561

This PDF file includes:

Methods

Fig. S1

Tables S1 to S5

References

Supporting Online Material

Analytical methods

Tables A1-A4 list the bulk, glass, core olivine and rim olivine compositions used in calculating the K_{DS} listed in Table 1 of the paper. All were measured by electron microprobe using Carnegie's JEOL JXA-8800L electron microprobe and the USGS's JEOL JXA-8900 microprobe. Both are equipped with five wavelength dispersive spectrometers (WDS). For all data reduction, the ZAF correction was used.

Olivine analyses were conducted with a 15 kV, 100 nA beam either as a focused spot or rastered over a 5x5 μm area. All elements were measured by WDS. To minimize the possibility of interferences affecting the Na analyses, a narrow pulse height analyzer energy window of 2 V centered on the Na peak was used and the background measurement positions, 2.1 mm on either side of the Na peak, were carefully chosen for regions where there should be no peaks from other elements in the olivine. In the absence of a suitable olivine standard, an augite standard was used for the Na calibration. Under these conditions and a total analysis time of 1600 s (800 s on the Na peak), a 3σ detection limit for Na in the olivine of ~ 26 ppm was achieved. Repeated analyses showed that olivine is stable against Na loss under these conditions. When possible, profiles across phenocrysts and the cores of olivine microphenocrysts (~ 10 μm) were measured, along with the compositions of the glass and clinopyroxene.

Clinopyroxene analyses were done using 15 kV and 20 nA beam current, with a focused beam. Analysis times were varied, from 60 s on the Na peak in clinopyroxene grains in type II chondrules to 1800 s for those in some type I chondrules. Five to ten areas of glass were measured in each chondrule, chosen to be as free of clinopyroxene crystallites as possible, and covering both the inner and outer parts of the chondrule. Glass analyses followed the procedure of Grossman and Brearley (1). This included a correction made for Na loss during analysis of glass in type II chondrules, which, for the conditions used, was $\sim 11\%$. Although this correction accounts for Na loss during our own analyses, we could not fully assess or correct for Na loss suffered during previous

analyses of our sections by other workers. Previous spot analyses of mesostasis would have depleted the area by at least a factor of 2 in Na, which would be revealed by a statistically low Na measurement relative to other points in the same chondrule. Several of these were encountered, and discarded. Previous x-ray mapping or other prolonged exposure to a scanning electron beam presents more of a problem, as this has the potential to deplete Na in mesostasis over a wide area; experience shows that typical x-ray mapping conditions (100 nA beam current and 20-30 ms dwell time per pixel) can deplete Na by at least 10%. Such artificial depletions would be difficult to detect.

Bulk compositions were measured by superimposing a 10×10 grid of analytical points over each chondrule. Each point was analyzed using a 10 μm wide rastered beam, at 15 kV accelerating voltage and 20 nA beam current. For these measurements, WDS was used for Na, Ti, Al, Mg, Mn, and K, and energy dispersive analysis was used for Si, Ca, Cr, Fe, P, Ni and S. The method had a total analytical time of 70 s for each spot. After analysis, each point was located using backscattered electron imagery, and those falling outside the chondrule border and on cracks or holes were discarded. Analyses with totals below 80% were also discarded, as were analyses that showed evidence for contamination with polishing compound ($\text{Al}_2\text{O}_3 > 3 \text{ wt}\%$, CaO and $\text{Na}_2\text{O} < 1 \text{ wt}\%$; a problem in one of our thin sections). FeO was recalculated by subtracting Fe to form FeS with any measured S. A correction was also made for Fe present as Fe-Ni metal. To do this, spot analyses of metal grains in each chondrule were done for Fe and Ni. FeO was again corrected by removing enough Fe to combine with measured Ni to form Fe-Ni of the appropriate composition. The resulting compositions, including FeO, FeS, and Fe-Ni were normalized to 100% to correct for small cracks, and an average was calculated for the entire chondrule.

Because the average compositions calculated for each chondrule are essentially a modal reconstruction, the data was corrected for the densities of glass, metal, troilite, olivine, and pyroxene contributing to the uncorrected bulk composition. The volume percent of modal glass was calculated by subtracting the average composition measured for mesostasis in each chondrule (Table A2) from the uncorrected bulk composition until either Na or Al, or in a few type I chondrules, Ca, was used up; usually Na and Al approached zero at nearly the same time during the calculation. The volume percent of

metal and troilite were taken to be their concentrations in the uncorrected bulk composition. The residuum after subtracting mesostasis, metal, and troilite was mainly the modal olivine plus pyroxene, and the olivine/pyroxene ratio could be calculated from the (MgO+FeO)/SiO₂ molar ratio. The volume percentages of all four phases were then converted to weight percentages on the basis of their densities. The density-corrected bulk composition was then calculated by multiplying the composition of each component by its weight fraction and summing. Because of larger uncertainties, occasionally low abundance elements concentrated in the glass, like K, would be negative in the residuum. In these case, the bulk K/Na ratios, for instance, were taken to be those of the glass. For P, in type IIs its bulk abundance was determined from its abundance in glass and in type Is from its abundance in metal.

Glass densities were estimated using the approach of (2, 3). First the density of a melt with the glass's composition was calculated at an estimate of the limiting fictive temperature using the data of (4). The limiting fictive temperature, T_f , is where melt and glass would have the same density. Then the glass density at room temperature was calculated using an estimate of its coefficient of thermal expansion (α). The values of T_f and α were estimated using the empirical functions $T_f = 1175.5 - 93.93R$ and $\alpha = 10^{-5}(1.877R + 0.5319)$, where R is the ratio of the mole fractions of network modifiers to network formers (e.g., $(X_{MgO} + X_{FeO} + X_{CaO} + 2X_{Na_2O}) / (X_{SiO_2} + X_{Al_2O_3} + X_{P_2O_5})$). This approach is able to reproduce the room temperature glass densities measured by (2) to within 1-2%. The density of olivine was calculated from the atomic Mg/(Mg+Fe) ratio of the calculated olivine and pyroxene component based on the data of (5). The density of pyroxene was estimated by interpolating between 3.2 and 3.95 g/cm³ for end-member enstatite and ferrosilite, respectively. The densities used for troilite and Fe-Ni were 4.61 and 7.95 g/cm³, respectively.

Assessing the bulk chondrule, mineral and glass compositions

Accurate analyses, particularly of Na in olivine, are essential to this study, but the measurements can potentially be compromised in a number of ways. For instance, olivine phenocrysts often contain inclusions, and near the edges of the grains there can be x-ray fluorescence of the adjacent glass or glass just below the surface of the section. These effects will compromise the analyses, especially for elements like Na with low abundances in the olivine and high abundances in the glass. Analyses of clinopyroxene can also be compromised in this way. Consequently, all olivine and clinopyroxene analyses were checked for stoichiometry. In addition, those analyses that differed markedly from the bulk of the analyses were rejected. Generally, in the olivine Na, Mg, Fe, Cr, Mn and Ca are correlated. As a further check, if any phenocryst and microphenocryst analyses fell off the correlation trends in the direction of the glass composition, they were also rejected. Finally, in type II chondrules Al contents are always low. Because even very minor ‘contamination’ of an olivine analysis by glass or inclusions can have a marked effect on Na abundances, only type II olivine analyses with Al₂O₃ contents <0.04 wt% were used. A number of analyses of phenocryst rims and microphenocrysts that were very close to the glass were rejected using this criterion, but it was deemed more important to have reliable Na contents than questionable analyses at the very edges of the grains.

Chondrules, particularly in Semarkona, can have radially zoned mesostasis compositions (6-8). This zonation is secondary, produced by an influx of alkalis, halogen and water after crystallization of clinopyroxene; it probably occurred on the parent body (6, 7). Glass compositions were measured at the edges and cores of the chondrules. If there was a significant difference between edge and core compositions, only the core compositions were used. When evidence for alkali zonation in the mesostasis was found, the Na contents of the bulk compositions were adjusted to give the same Na/Al ratios as those of the core glasses.

A final complication in the analysis of glass in type II chondrules is caused by the segregation of alkalis into two separate phases, albitic feldspar and a more K-rich glass (Grossman and Brearley, 2005). The glass has a Na/K ratio fairly close to chondritic and represents the original mesostasis at the end of crystallization; the albite frequently has Na/K >20×CI, and was likely formed after the solidification of the chondrule. Fifty

percent of the type II chondrules in this study contained albitic regions in the mesostasis. Any analyses of glass that were high in Na and had anomalously high Na/K were discarded.

Clinopyroxene and the initial compositions of chondrule glasses

Even in the chondrules with no alkali radial zonation in their glass, the high mobility of Na means it is possible that they have not remained closed to Na since formation. The Na₂O contents in clinopyroxene and glass in our chondrules resemble those reported in previous studies (6, 9) – for type Is $K_D \approx 0.04$ lines, while the K_D s for most type IIs are significantly higher and more variable. The late crystallizing clinopyroxene in chondrules offers a means to test whether there has been post-crystallization entry of Na into chondrules.

Previously, it was shown that the good correlation between clinopyroxene and glass Na contents in type I chondrules are consistent with clinopyroxene crystallizing from melts with Na contents like that of the current mesostases at temperatures of ≥ 1573 K (6, 9, 10). This temperature is roughly consistent with clinopyroxene crystallization temperatures predicted by MELTS. In type II chondrules, Na in clinopyroxene and glass are not well correlated. This lack of correlation is expected if the clinopyroxene in type IIs typically formed at lower temperatures than in type Is because the Na clinopyroxene-melt K_D becomes more temperature sensitive below ~ 1573 K (6). While we cannot rule out some loss or gain of Na in type II chondrules, the clinopyroxene-glass K_D s suggest that the Na contents of most chondrule glasses (excluding the outer regions of zoned chondrules) were set at the time of the final crystallization of the chondrules.

Assumptions and sources of error in the calculation of K_D s.

A number of assumptions go into estimating the K_D s. For estimating the rim K_D s from the phenocrysts' rims and from microphenocrysts, it is necessary to assume that: (i) the glass has not experienced any change in Na content since solidification, and (ii) the olivines measured were in equilibrium with the glass. The clinopyroxene compositions

suggest that the glasses in most of the chondrules resemble the final melt compositions. However, Na is quite mobile in chondrule glasses, particularly in type IIs, and loss or gain of Na after solidification could account for the distribution of chondrules along the 1:1 line in Figure 2. Some Na loss could even have occurred during analyses of our sections by earlier workers.

It is difficult to demonstrate that the olivines that were measured were in equilibrium with the final melt. They are the most extreme compositions we were able to obtain for each chondrule that met the criteria listed above. However, it is not possible to analyze the olivine directly in contact with the glass because fluorescence of the glass will lead to anomalously high Na contents. It is likely that there was some clinopyroxene and olivine growth after the measured olivines crystallized. Therefore, the reported rim K_{DS} should be regarded as lower limits. The pyroxene-bearing chondrules are particularly variable in the ratios of their core/rim K_{DS} (Table 1 and Fig. 2), possibly because olivine ceased crystallizing or was dissolving while the pyroxene was crystallizing, and so the olivine phenocryst rims were not in equilibrium with the observed glass.

For the core K_D estimates, the necessary assumptions are that: (i) the chondrules were full molten when they formed, (ii) that the most extreme core composition in the section of a chondrule reflects the composition of the first material to crystallize, (iii) that there was little re-equilibration during crystallization, (iv) that relict cores can always be recognized and avoided, (v) that the chondrules have remained closed to Na loss or gain since their initial melting, and (vi) that the estimated bulk compositions resemble the true ones (i.e., the sections of the chondrules are representative of the whole, and the grid sampling was unbiased).

All but two of the chondrules analyzed have porphyritic textures. C33 is a barred olivine type II chondrule and was therefore entirely molten. C6 is a type I chondrule that also has olivine bars in its core. Experiments show that to develop porphyritic textures requires that some nuclei survive melting, but these nuclei could be much smaller than the resolution of our instruments. Thus, it is entirely possible that the porphyritic chondrules were essentially completely molten. Nevertheless, it cannot be ruled out that some of the cores are unmelted relicts with similar major element compositions to the surrounding olivine, making them difficult to recognize. Recognizing relict cores is

particularly problematic in type Is. Many of the phenocryst cores in the type Is studied had somewhat higher FeO contents than the rims. This and the high core K_{DS} in the type Is could be the result of loss of Na and increasingly reducing conditions during cooling. However, it could also mean that most of the cores are relict.

Olivine compositions do not change much in the early stages of crystallization. Consequently, although it is unlikely that any of the sections of the phenocrysts have passed directly through their centers, as long as one or more section in each chondrule passed close to the center, assumption (ii) will be valid.

The preservation of zoning in phenocrysts, particularly those with relict cores, suggests that there was little re-equilibration during crystallization. However, for many chondrules the core compositions are not as Mg-rich as the first predicted by MELTS using the estimated bulk compositions. This could reflect uncertainties in MELTS for these compositions and errors in the assumed fO_2 during crystallization, but it is possible that the measured cores do not represent the very first crystallites, perhaps because near equilibrium was maintained while the crystallites were small.

Calculation of olivine zonation in Figure 1

The two Na zonation curves in Figure 1 of the paper illustrate what would be expected for closed system crystallization and for formation in the nebula with solids densities that until now were considered very high.

The closed system curve was calculated using the bulk composition of chondrule C3 and progressively extracting olivine from it. The Na content of the olivine at each step was calculated using the Na content of the residual melt and a K_D of 0.0075. This K_D is intermediate between the core and rim K_{DS} measured for chondrule C3 (Table 1). The final mass of olivine was assumed to form 60 μm phenocrysts, allowing for calculation of the radial zonation from the mass fraction of olivine that had crystallized at each step.

To model open system formation in the nebula, we calculated the equilibrium mineral, melt and gas compositions at 10 K intervals from 2000 K, when olivine first appears, to 1140 K. The only silicate phases that were allowed to form were olivine, pyroxene (ortho- and clino-) and silicate melt. The total pressure of the nebula gas was assumed to

be 10^{-3} bars, and the system was enriched 1000 times in CI-composition solids relative to the solar abundance. The predicted radial zonation was calculated as above from the fraction of olivine that had crystallized and the Na content of the melt at every temperature interval. Sodium is confined to the rim of the model phenocryst because it only begins to reside in the melt in significant amounts below 1600 K, while the olivine has already been crystallizing for more than 400 K of cooling. At its center, the predicted phenocryst has what, in terms of Fe/Mg ratio, resembles a relict core. However, this is probably not how relict cores form. While common, relict cores are not ubiquitous in type II chondrules, and the Na zoning around the relict cores is quite different from what is predicted.

Calculation of chondrule equilibrium vapor pressures and solids densities

The equilibrium Na vapor pressure (p_{Na}) over a chondrule is determined by the reaction $\text{Na}_2\text{O}_{(l)} = 2\text{Na}_{(g)} + \frac{1}{2} \text{O}_2$. Hence, the ambient f_{O_2} largely dictates the Na vapor pressure of a chondrule – the higher the f_{O_2} , the lower the p_{Na} . There is some uncertainty in what controlled the f_{O_2} during chondrule formation, particularly for the type IIs. Consequently, we calculated the equilibrium vapor pressures in two ways to cover the likely extremes in the f_{O_2} . In the first approach, the equilibrium vapor pressures of the chondrules were calculated using the approach of (11, 12) assuming that only silicates were present (i.e., there was no metal present to buffer the f_{O_2}). Na_2O and P_2O_5 largely dictate the f_{O_2} under these conditions, and the f_{O_2} can be orders of magnitude above the iron-wüstite buffer. At such high f_{O_2} s, one might expect significant Fe^{3+} to be present in chondrules, but primary Fe^{3+} -bearing minerals have not been reported in chondrules. Thus, this approach represents the most oxidizing conditions that could have existed during chondrule formation. If H_2 was present during chondrule formation, as would have been the case if chondrules formed in the nebula, this will depress the f_{O_2} and increase the p_{Na} .

If metal was present during chondrule formation, as appears to be the case for most chondrules, it will buffer the f_{O_2} through reaction with FeO in the melt. At least small amounts of metal and sulfide are present in all the chondrules studied (Table A1). However, it is not clear to what extent the metal and sulfide have been affected by

secondary processing. Also, because metal and sulfide will form a single melt at high temperature, it is necessary to accurately determine the metal/ sulfide ratio. This is not always easy to do. Because of these potential ambiguities, rather than use the measured metal/sulfide compositions, in the second approach we assumed that chondrules equilibrated with pure Fe-metal. This results in the lowest f_{O_2S} that were likely to have existed during chondrule formation.

The solids densities required to approximate closed-system behavior were estimated by calculating, for a given temperature and partial pressure of Na, the density of solids required for 90% of the Na to remain condensed. In this case, the solid density, S (g/m^3), is given by

$$S = \frac{P_{Na} M_{Na} f_{Na}}{(1 - f_{Na}) R T X_{Na}}, \quad (1)$$

where P_{Na} is the equilibrium Na vapor pressure of the chondrule (N/m^2), M_{Na} the molar weight (g/mole) of Na, X_{Na} the mass fraction of Na in the chondrules, f_{Na} if the fraction of Na in the system in chondrules, R the gas constant (J/mole/K) and T the temperature (K).

While in the paper we concentrate on the solids densities at liquidus temperatures, the roughly closed system behavior of Na places constraints on solids densities over the entire temperature interval of crystallization. These constraints are important if a chondrule formation model predicts changing solids densities with time and temperature. For instance, in shock models there is significant pre-shock heating of chondrule precursors at much lower solids densities than in the higher temperature post-shock region. Unless there is efficient Na recondensation in the post-shock region prior to the onset of crystallization, the solids densities in the pre-shock region must be high enough to suppress Na evaporation during pre-shock heating.

To illustrate the constraints as a function of temperature, we have calculated the equilibrium vapor pressures in the same way as above for representative type IA and IIA chondrule compositions (Table A5) as they crystallize (Fig. A1). For the silicates-only calculations, we have made additional calculations assuming constant partial pressures of

H_2 (p_{H_2}) of 10^{-8} , 10^{-6} and 10^{-4} bars. At $p_{H_2}=10^{-8}$ bars, the result is essentially that for a H_2 -free system.

How might such high chondrule concentrations be achieved?

Producing the high spatial concentrations of chondrules estimated in this work is a challenge for models of dust dynamics in protoplanetary disks. In a non-turbulent disk small particles are able to settle to the midplane, but once their density approaches that of the gas ($\sim 200\times$ solar), shear between this particle-enriched layer and the gas above it would lead to the development of localized turbulence (15). This turbulence would then loft particles to higher altitudes. This is a self-regulating mechanism that limits the enhancement of solids around the midplane to less than 200. This barrier can be breached if the solids decouple from the gas by growing much larger in size, but such particles would be too large to be chondrule precursors. Obviously, other sources of turbulence will also limit the solid concentrations that settling can achieve.

It is important to note that these studies have largely focused on global increases of solids at the midplane. There are proposed mechanisms that would create much larger enhancements in localized regions of the nebula. One such mechanism, turbulent concentration (16), would allow chondrule-sized particles to concentrate in very dense regions of the nebula if the turbulence parameter ranged between $\alpha=10^{-5}$ to 10^{-3} . The concentrations that would be produced range up to $\square 10^6$ times greater than solar. The small concentrations would be the most common, whereas the very high concentrations would be rare and occupy relatively small volumes of the disk (16). As mass loading at very high concentrations (mass enhancements of $\square 10^5$) develop, the turbulence decays away, resulting in a locally less turbulent region of the disk (17).

It has also been proposed that if the concentration of solids in a particular region of the nebula was high enough, it would be stable against the turbulence that had been predicted to develop as a result of the shear instabilities described above, with (18) arguing that the column density of small solids (chondrule-sized and smaller) must be enhanced by factors of 2 to 10 above the canonical abundance for this effect to occur. This still requires significant settling of the particles to the disk midplane, and thus requires global turbulence to be minor ($\alpha < 10^{-7}$ according to (18)).

Similarly, (19) demonstrated that very large concentrations of particles (enough to form planetesimals the size of Ceres) could develop in disks in which the magnetorotational instability operates as a result of transient pressure gradients that develop within the disk. These studies, however, focused on solids much larger than chondrule-precursors as this produced favorable aerodynamic properties for the particular cases considered. Whether chondrule precursors could similarly be concentrated at lower gas densities (for example) remains to be determined.

Thus, there are ways by which large enhancements of chondrules could be produced at least locally in the solar nebula, though it is important to stress these means must still be studied in more detail before they are universally accepted as plausible. In all cases, it is important to note that concentrations of the type found here would be very rare in the nebula. Thus if there is a causal link between chondrule and planetesimal formation, this could explain how dust (chondrule precursors) was sustained in the nebula over long timescales, whereas most models of planetesimal formation suggest that their formation would take place very rapidly.

Estimating the sizes of self-gravitating regions in a turbulent nebula.

For a region of high chondrule density to become self-gravitating, the escape velocity of chondrules at the surface of the region must be greater than their random velocities. Defining the escape velocity as the typical velocity at which the kinetic energy of a chondrule equals its gravitational potential energy gives

$$\frac{1}{2}m_c v^2 = \frac{GMm_c}{R}, \quad (2)$$

where m_c is the mass of a chondrule, M is the mass of the region, R is the radius of the region, v is the escape velocity at the surface of the region and G is the gravitational constant. The mass of the region with a density, ρ , is given by

$$M = \frac{4}{3}\pi R^3 \rho. \quad (3)$$

Combining equations 2 and 3, the escape velocity is

$$v = R\sqrt{\frac{8}{3}\pi G\rho}. \quad (4)$$

In a turbulent disk, it will be the velocities induced by the random motions of the gas that must be less than the escape velocity. High chondrule densities may damp turbulent motions of the gas. Nevertheless, taking the upper limit for the random chondrule velocity as that of the undamped gas (20) and setting it equal to the escape velocity, we have

$$v = c\sqrt{\alpha} = R\sqrt{\frac{8}{3}\pi G\rho}, \quad (5)$$

where c is the sound speed in the gas and α the dimensionless viscous disk parameter. Rearranging, the critical density for a region becomes

$$\rho_{crit} = \frac{3\alpha c^2}{8\pi GR^2}. \quad (6)$$

Assuming typical values of $\alpha=10^{-4}$ and $c=1000$ m/s, and a chondrule density of 10 g/m³, similar to the lower limit estimates for near liquidus densities in Table 1 and Figure A1, regions >4000 km in radius will be self-gravitating. To be conservative, the value of α assumed here is higher than discussed earlier, but it is typical of the values used to characterize the solar nebula and for matching some aspects of meteorites (16, 17). Of course, if the value of α was lower than this where chondrule/chondrite formed, self-gravitating regions will be smaller for a given density. The sound speed is appropriate for a gas at a few hundred Kelvin, so these sizes apply to when the regions have cooled. If turbulence was much lower, as discussed above, and/or densities much higher, even smaller regions could become self-gravitating.

Estimation of cooling rates and timescales

In estimating the cooling rate of a region with the high chondrule densities calculated here, we adopted two different approaches. In the first, we treated the region as being the equivalent of a uniform (isothermal at temperature T and constant density of ρ) sphere of radius, R . The sphere cools by radiating energy from its surface at a rate of $4\pi R^2 \sigma T^4$, with σ being the Stefan-Boltzmann constant and C_p the heat capacity of the sphere, while its total energy is given by $(4/3) \pi R^3 \rho C_p T$. We assume the density and heat capacity were dominated by the chondrules and ignore the effects of the gas. The cooling rate is thus given by:

$$\frac{dT}{dt} = \frac{3\sigma T^4}{\rho C_p R}. \quad (7)$$

For $\rho = 10 \text{ g/m}^3$, $R = 4000 \text{ km}$ and $C_p = 1000 \text{ J/kg/K}$, the cooling rate at 2000 K would be $\sim 250 \text{ K/hr}$ and at 1500 K would be $\sim 30 \text{ K/hr}$. These rates are consistent with cooling rates inferred for chondrules. Of course, in a natural system cooling rates will vary with radial distance from the center of the region. Nevertheless, the important conclusion of these simplistic estimates are that for the sizes and densities of the regions inferred above, the cooling rates would be of the right order for chondrules.

We can also calculate the thermal adjustment timescale for a spherical region, defined as the time for it to achieve radiative equilibrium with the surrounding medium. This timescale is given by (21):

$$t_{rad} = \frac{\rho^2 \kappa C_p R^2}{64 \sigma T^3}, \quad (8)$$

where κ is the opacity of the medium ($\sim 5 \text{ cm}^2/\text{g}$ for chondrules) and all other terms are defined as above. Using the same parameters as above, the thermal adjustment timescale for a region at 2000 K is $\sim 2.8 \times 10^7$ seconds or ~ 1 year. Even though the exact cooling history will depend on the temperature of the system, the timescale computed here is

much longer than the estimated duration of chondrule formation based on cooling rates. However, the cooling rates only apply to the high temperature epoch (>1500 K). The thermal adjustment timescale is more appropriate to the minimum time that must elapse between chondrule formation and the introduction of low temperature matrix material to the region and final chondrite assembly.

Mixing of matrix, CAIs and chondrules

If the chondrule formation regions were gravitationally bound and could, possibly, directly collapse to form the meteorite parent bodies, we must ask how materials found in chondritic meteorites that were not processed in chondrule forming events (e.g., pre-solar materials, volatile-rich matrix material, and unmelted CAIs) can be intimately mixed in these bodies. Below we outline one plausible scenario.

Once a gravitationally bound clump forms it will tend to contract, but the pressure of the gas in the clump will provide some resistance to inward motions. This significantly increases the timescales for contraction of these bodies as the solids have to settle more slowly to the center of the clump through the gas. The contraction time, dictated by the settling time of the chondrules (17), is estimated to be given by:

$$t = \frac{\rho_g c}{4G\rho_c r \rho_s}, \quad (9)$$

where ρ_g is the local density of the gas, c the local sound speed, r the radius of the particles, ρ_c is the density of the clump and ρ_s the internal density of the particles. Assuming typical parameters of $c = 10^3$ cm/s, $\rho_s = 3$ g/cm³, $r = 0.05$ cm, $\rho_c = 10^{-5}$ g/cm³ as in this work, we find that $t = 8-80$ years for $\rho_g = 10^{-9} - 10^{-8}$ g/cm³ respectively, or $\square 1-15$ orbits at 3 AU.

Assuming the diffusivity of small grains in a turbulent gas (see 20), a particle could travel a distance of

$$x(km) = 9000 \left(\frac{\alpha}{10^{-7}} \right)^{1/2} \left(\frac{t}{1yr} \right)^{1/2} . \quad (10)$$

Even at very low levels of turbulence ($\alpha < 10^{-7}$), a particle could diffuse 25,000 km over an 8 year period (3 times that over an 80 year period). This is greater than the scale of the chondrule formation region estimated by (22).

Thus we arrive at a picture of chondrule formation being restricted to occur in very small regions of the nebula with very high densities of solids. Given the high densities of solids, it is likely that whatever event was responsible for chondrule formation would have processed solids in that region to a different extent than materials further away. For example, as discussed in (23), there is significant feedback on the gas by the solids if chondrules form via shockwaves allowing higher temperatures to be reached at high chondrule concentrations than would be otherwise. Thus a low velocity shock ($\approx 2-3$ km/s) could suffice to melt the chondrules in the very dense clump, but minimally process materials outside the clump, allowing pre-solar grains or CAIs located thousands to ten thousands of kilometers away to show no signs of thermal processing. If the chondrules then become gravitationally bound after their processing (due in part to the increased density that accompanies processing in shock waves) they will contract on timescales of a few orbits. This would allow the unprocessed materials to diffuse into the self-gravitating clump before it completely collapses.

We stress this scenario requires detailed testing, but it is consistent with our current understanding of chondrule formation and mixing in protoplanetary disks. Future work should address the specific details of dust grains diffusing into self-gravitating clumps.

References

1. J. N. Grossman, A. J. Brearley, *Meteoritics Planet. Sci.* **40**, 87 (2005).
2. R. A. Lange, *Contrib. Mineral. Petrol.* **130**, 1 (1997).
3. J. A. Tangeman, R. A. Lange, *Am. Mineral.* **86**, 1331 (2001).
4. R. A. Lange, I. S. E. Carmichael, *Geochim. Cosmochim. Acta* **51**, 2931 (1987).
5. G. W. Fisher, L. G. Medaris Jr., *Am. Mineral.* **54**, 741 (1969).
6. C. M. O'D. Alexander, J. N. Grossman, *Meteoritics Planet. Sci.* **40**, 541 (2005).
7. J. N. Grossman, C. M. O'D. Alexander, J. Wang, A. J. Brearley, *Meteoritics Planet. Sci.* **37**, 49 (2002).

8. S. Matsunami *et al.*, *Geochim. Cosmochim. Acta* **57**, 2101 (1993).
9. G. Libourel, A. N. Krot, I. Tissandier, *Lunar Planet. Sci.* **XXXIV**, #1558 (abstr.) (2003).
10. R. H. Jones, *Geochim. Cosmochim. Acta* **58**, 5325 (1994).
11. D. S. Ebel, *Geochim. Cosmochim. Acta* **69**, 3183 (2005).
12. D. S. Ebel, L. Grossman, *Geochim. Cosmochim. Acta* **64**, 339 (2000).
13. R. H. Jones, E. R. D. Scott, *Proc. 19th Lunar and Planetary Science Conference*, 523 (1989).
14. R. H. Jones, *Geochim. Cosmochim. Acta* **54**, 1785 (1990).
15. S. J. Weidenschilling, *Icarus* **181**, 572 (2006).
16. J. N. Cuzzi, R. C. Hogan, J. M. Paque, A. R. Dobrovolskis, *Astrophys. J.* **546**, 496 (2001).
17. J. Cuzzi, R. C. Hogan, K. Shariff, *Astrophys. J.*, In press (2008).
18. A. N. Youdin, F. H. Shu, *Astrophys. J.* **580**, 494 (2002).
19. A. Johansen *et al.*, *Nature* **448**, 1022 (2007).
20. J. N. Cuzzi, S. J. Weidenschilling, in *Meteorites and the Early Solar System II*, D. S. Lauretta, H. Y. McSween, Jr., Eds. (University of Arizona Press, Tucson, 2006), pp. 353-381.
21. R. Kippenhahn, A. Weigert, *Stellar Structure and Evolution* (Springer-Verlag, New York, 1996), pp. 468.
22. J. N. Cuzzi, C. M. O'D. Alexander, *Nature* **441**, 483 (2006).
23. F. J. Ciesla, L. L. Hood, *Icarus* **158**, 281 (2002).

Any use of trade, product, or firm names is for descriptive purposes only and does not imply endorsement by the U.S. government.

Fig. A1. The solids densities necessary for 90% of the Na to remain in (a) type IIA and (b) type IA chondrules rather than be lost to the gas. As described in the text, to estimate the range of possible densities required, the densities were calculated using the Na partial pressures in the equilibrium vapor over the chondrules assuming: (i) three constant partial pressures of H₂ (10⁻⁸, 10⁻⁶ and 10⁻⁴ bars), and (ii) that the fO₂ of the vapors were buffered by equilibrium between FeO in the melt and pure Fe-metal.

Table A1. The bulk compositions (wt%) determined for the Semarkona chondrules studied.

	Na ₂ O	MgO	Al ₂ O ₃	SiO ₂	P ₂ O ₅	K ₂ O	CaO	TiO ₂	Cr ₂ O ₃	MnO	FeO	FeS	Ni	Fe	Total
C1	1.16	32.40	2.33	42.11	0.43	0.12	2.13	0.11	0.53	0.39	17.09	0.24	0.33	0.66	100.03
C2	1.44	31.00	3.01	45.21	0.05	0.18	3.24	0.14	0.62	0.43	12.54	0.42	0.49	1.20	99.95
C3	0.94	30.78	2.52	42.10	0.37	0.14	2.19	0.11	0.47	0.39	19.08	0.38	0.47	0.24	100.20
C4	0.65	35.01	1.83	44.23	0.05	0.13	2.13	0.08	0.53	0.42	12.94	0.17	0.36	1.67	100.22
C5	0.87	28.89	2.17	40.30	0.27	0.12	2.12	0.09	0.40	0.40	21.35	1.74	0.51	0.77	99.99
C6	0.18	38.94	6.30	45.70	0.12	0.02	6.14	0.31	0.26	0.09	0.53	0.11	0.52	0.96	100.19
C7	0.65	39.09	6.65	44.53	0.09	0.03	5.36	0.32	0.40	0.14	0.47	0.20	0.56	1.69	100.17
C8	0.17	41.96	4.52	45.52	0.08	0.03	3.43	0.16	0.51	0.16	0.74	0.23	0.32	2.27	100.11
C9	0.08	43.32	2.84	45.53	0.16	0.03	2.32	0.13	0.35	0.07	0.73	0.16	0.67	3.79	100.16
C10	1.32	29.52	3.33	42.08	0.46	0.13	3.00	0.12	0.59	0.38	17.20	0.94	0.32	0.51	99.90
C11	0.05	40.60	4.40	39.78	0.11	0.02	2.82	0.14	0.46	0.09	0.67	0.42	0.92	9.65	100.12
C13	1.96	23.95	3.89	43.92	0.11	0.23	2.80	0.17	0.49	0.46	15.06	2.74	0.54	3.68	100.02
C14	1.38	30.77	2.79	42.83	0.18	0.13	2.66	0.11	0.42	0.37	15.65	1.83	0.43	0.25	99.81
C18	1.54	28.93	2.92	41.35	0.12	0.14	2.01	0.10	0.60	0.45	17.82	2.14	0.80	1.08	100.00
C19	1.34	31.13	4.25	48.93	0.05	0.13	2.41	0.14	0.60	0.56	6.76	0.38	0.56	2.65	99.89
C20	1.05	36.73	2.54	44.39	0.06	0.13	2.42	0.10	0.56	0.44	10.41	0.21	0.31	0.62	99.97
C22	1.36	32.16	3.39	43.11	0.30	0.15	2.46	0.11	0.57	0.42	13.00	1.14	0.61	1.23	100.03
C23	1.51	27.83	3.28	40.49	0.21	0.12	2.55	0.11	0.48	0.41	18.87	2.03	0.63	1.26	99.80
C27	0.85	33.09	2.27	46.91	0.07	0.08	1.94	0.09	0.63	0.48	10.90	0.26	0.41	1.97	99.94
C29	1.81	27.05	2.99	44.76	0.06	0.24	3.27	0.12	0.68	0.54	12.87	3.82	0.50	1.00	99.71
C31	1.09	29.23	2.28	46.10	0.06	0.10	1.83	0.09	0.65	0.51	15.76	0.47	0.44	1.27	99.86
C33	1.65	28.81	3.61	42.60	0.55	0.19	3.65	0.16	0.58	0.55	15.46	1.18	0.40	0.40	99.78
C34	2.16	21.43	3.98	40.33	0.57	0.22	2.88	0.14	0.54	0.42	16.11	4.68	1.23	5.24	99.92
C35	1.79	25.09	3.90	41.74	0.56	0.20	3.01	0.14	0.50	0.39	19.74	1.67	0.72	0.37	99.82
C38	0.99	34.44	2.54	41.04	0.54	0.12	3.02	0.12	0.51	0.45	14.05	0.48	0.50	1.00	99.80
C40 ¹	0.45	29.85	1.90	50.60	0.11	0.08	1.01	0.06	0.61	0.59	13.85	0.53	0.18	0.37	100.18

¹Not density corrected because good mesostasis analyses were not obtained.

Table A2. The average glass compositions (wt%) for the chondrules studied.

	Na ₂ O	MgO	Al ₂ O ₃	SiO ₂	P ₂ O ₅	K ₂ O	CaO	TiO ₂	Cr ₂ O ₃	MnO	FeO	Total
C1	4.88	2.27	12.09	63.77	1.89	0.55	5.96	0.48	0.08	0.20	6.85	99.01
C2	5.94	1.62	13.37	70.41	0.23	0.92	1.47	0.51	0.07	0.24	5.97	100.76
C3	4.52	3.43	12.55	62.66	1.69	0.76	4.93	0.44	0.06	0.16	6.08	97.26
C4	3.91	1.68	11.04	70.93	1.40	0.90	0.57	0.53	0.03	0.18	6.54	97.71
C5	5.65	1.06	14.64	69.12	1.25	0.89	2.88	0.51	0.04	0.07	3.29	99.41
C6	0.57	5.81	19.76	54.66	0.01	0.01	15.66	0.92	0.46	0.14	0.35	98.35
C7	1.43	3.35	14.13	67.88	0.00	0.08	9.87	1.11	0.41	0.33	0.56	99.14
C8	0.81	5.58	18.13	57.73	0.02	0.03	14.49	0.76	0.58	0.24	0.38	98.76
C9	0.44	6.03	18.38	56.39	0.01	0.03	15.16	0.60	0.47	0.10	0.37	98.00
C10	5.87	2.70	12.49	65.58	0.68	0.70	4.50	0.56	0.22	0.17	6.53	99.99
C11	0.25	6.61	23.20	50.47	0.01	0.00	15.74	1.13	0.60	0.10	0.46	98.57
C13	6.82	0.75	14.21	73.57	0.31	1.00	0.57	0.53	0.03	0.09	4.14	102.02
C14	6.64	2.78	13.33	66.41	0.74	0.65	2.56	0.44	0.07	0.19	7.98	101.80
C18	6.72	0.68	14.87	71.78	0.28	1.00	0.62	0.53	0.01	0.11	3.94	100.53
C19	8.45	1.50	16.37	67.26	0.09	0.79	2.11	0.59	0.03	0.32	4.41	101.94
C20	5.92	2.25	12.03	72.37	0.21	0.89	0.81	0.48	0.08	0.22	5.14	100.40
C22	6.54	2.51	11.20	67.23	1.38	0.74	1.53	0.51	0.05	0.32	8.26	100.27
C23	6.93	2.77	14.32	69.03	0.67	0.92	1.94	0.43	0.09	0.12	4.68	101.90
C27	7.77	1.14	16.09	69.79	0.25	0.94	0.80	0.56	0.04	0.17	3.89	101.44
C29	10.18	1.32	15.75	67.80	0.04	0.38	1.19	0.36	0.07	0.12	3.32	100.54
C31	7.47	1.10	14.28	69.99	0.25	0.88	0.81	0.56	0.05	0.22	6.92	102.53
C33	7.33	4.94	9.30	68.49	0.76	0.64	1.11	0.38	0.05	0.41	8.42	101.83
C34	5.88	2.58	13.95	65.57	1.86	0.80	3.05	0.56	0.09	0.16	6.32	100.82
C35	5.05	3.06	11.44	63.95	1.46	0.70	7.50	0.56	0.16	0.16	7.32	101.35
C38	6.07	2.15	10.45	71.66	0.26	0.83	0.55	0.42	0.04	0.34	8.57	101.34

Table A3. The most Na- and Fe- poor core olivine compositions (wt%) for the chondrules studied.

	Na ₂ O	MgO	Al ₂ O ₃	SiO ₂	P ₂ O ₅	CaO	Cr ₂ O ₃	MnO	FeO	Total
C1	0.0090	50.33	0.03	40.64	0.00	0.11	0.28	0.22	10.20	101.83
C2	0.0041	47.26	0.03	39.71	0.02	0.11	0.42	0.26	10.59	98.41
C3	0.0090	48.22	0.03	38.96	0.09	0.12	0.27	0.21	9.72	97.65
C4	0.0050	48.15	0.02	39.40	0.03	0.09	0.30	0.24	9.00	97.25
C5	0.0133	40.50	0.02	37.61	0.03	0.15	0.42	0.32	18.92	98.02
C6	0.0035	55.00	0.16	41.12	0.00	0.40	0.16	0.02	0.55	97.44
C7	0.0007	55.35	0.36	41.21	0.00	0.50	0.11	0.01	0.35	97.96
C8	0.0012	55.01	0.07	40.34	0.00	0.25	0.27	0.05	0.61	96.62
C9	0.0021	54.18	0.08	40.84	0.00	0.25	0.23	0.03	0.66	96.30
C11	0.0039	53.92	0.04	38.68	0.00	0.30	0.23	0.03	0.65	93.89
C13	0.0060	44.97	0.04	39.74	0.01	0.09	0.40	0.34	14.56	100.19
C14	0.0045	49.35	0.04	40.01	0.02	0.10	0.27	0.20	8.77	98.78
C18	0.0050	44.37	0.02	38.84	0.01	0.09	0.47	0.40	15.04	99.23
C19	0.0012	50.98	0.02	40.04	0.00	0.07	0.34	0.25	6.16	97.89
C20	0.0043	50.77	0.04	40.73	0.01	0.09	0.36	0.26	7.56	99.85
C22	0.0080	49.43	0.03	40.06	0.01	0.11	0.34	0.25	8.75	98.98
C23	0.0022	46.57	0.02	39.42	0.05	0.08	0.35	0.21	11.86	98.58
C27	0.0052	47.09	0.02	40.07	0.00	0.10	0.42	0.36	11.96	100.04
C29	0.0017	46.55	0.03	39.43	0.00	0.08	0.46	0.39	12.25	99.21
C31	0.0066	45.43	0.03	39.95	0.03	0.10	0.39	0.34	14.37	100.68
C33	0.0041	45.78	0.02	40.02	0.00	0.09	0.34	0.33	13.92	100.53
C35	0.0105	44.37	0.04	39.23	0.04	0.16	0.45	0.31	15.63	100.26
C38	0.0035	45.96	0.03	37.94	0.01	0.10	0.41	0.34	12.63	97.42
C40	0.0026	45.68	0.02	39.02	0.02	0.06	0.45	0.43	13.50	99.20

Table A4. The most Na- and Fe-rich rim and microphenocryst olivine compositions (wt%) for the chondrules studied.

	Na ₂ O	MgO	Al ₂ O ₃	SiO ₂	P ₂ O ₅	CaO	Cr ₂ O ₃	MnO	FeO	Total
C1	0.0330	36.00	0.03	37.72	0.00	0.38	0.47	0.62	27.65	102.91
C2	0.0167	40.56	0.02	38.08	0.06	0.26	0.67	0.55	18.54	98.78
C3	0.0284	35.51	0.03	36.46	0.20	0.36	0.49	0.50	25.10	98.71
C4	0.0240	38.68	0.01	38.04	0.02	0.21	0.69	0.61	20.46	98.76
C5	0.0298	35.51	0.02	36.26	0.10	0.28	0.52	0.46	24.41	97.62
C6	0.0031	55.35	0.16	41.36	0.00	0.43	0.18	0.02	0.52	98.06
C7	0.0033	55.30	0.17	41.18	0.00	0.38	0.23	0.05	0.55	97.91
C8	0.0020	55.13	0.11	40.62	0.00	0.33	0.25	0.04	0.62	97.15
C9	0.0036	54.53	0.14	41.15	0.00	0.27	0.30	0.04	0.65	97.14
C10	0.0359	41.74	0.04	38.22	0.05	0.24	0.61	0.53	19.63	101.13
C11	0.0016	53.99	0.07	38.77	0.00	0.30	0.34	0.08	0.77	94.37
C13	0.0312	30.93	0.02	36.05	0.03	0.30	0.29	0.72	30.10	98.52
C14	0.0276	32.64	0.03	35.86	0.45	0.24	0.34	0.60	28.06	98.26
C18	0.0132	38.65	0.02	37.85	0.04	0.21	0.50	0.55	21.06	98.91
C19	0.0072	46.48	0.02	39.29	0.00	0.19	0.61	0.62	10.47	97.71
C20	0.0181	39.49	0.03	37.90	0.01	0.24	0.61	0.76	18.11	97.18
C22	0.0353	32.96	0.03	36.32	0.17	0.28	0.39	0.79	26.68	97.68
C23	0.0214	33.77	0.03	35.05	0.09	0.32	0.41	0.60	27.07	97.38
C27	0.0105	39.32	0.03	37.70	0.01	0.23	0.49	0.65	19.78	98.23
C29	0.0035	43.98	0.02	38.67	0.00	0.10	0.52	0.53	14.94	98.78
C31	0.0148	34.55	0.02	37.67	0.01	0.24	0.43	0.77	26.87	100.62
C33	0.0201	40.13	0.02	37.81	0.01	0.21	0.52	0.63	17.28	96.64
C34 ¹	0.0193	37.35	0.07	37.24	0.11	0.30	0.37	0.49	23.63	99.62
C35	0.0239	38.11	0.04	38.12	0.24	0.28	0.51	0.46	23.27	101.08
C38	0.0166	41.40	0.03	38.49	0.03	0.21	0.62	0.55	16.96	98.32

¹The Al₂O₃ content of this is higher than our criteria of 0.04 wt% for type II chondrules, but no better analysis could be obtained.

Table A5. The compositions used to calculate chondrule vapor pressures (From 13, 14).

	Type II A	Type IA
SiO ₂	45.72	46.96
TiO ₂	0.11	0.20
Al ₂ O ₃	2.72	4.09
Cr ₂ O ₃	0.52	0.46
FeO	15.06	1.24
MnO	0.40	0.13
MgO	31.71	42.63
CaO	1.92	3.67
Na ₂ O	1.67	0.54
K ₂ O	0.17	0.07